

A regularized higher-order beam elements for damage analysis of reinforced concrete beams

Original

A regularized higher-order beam elements for damage analysis of reinforced concrete beams / Shen, J.; Arruda, M. R. T.; Pagani, A.; Carrera, E.. - In: MECHANICS OF ADVANCED MATERIALS AND STRUCTURES. - ISSN 1537-6494. - 31:1(2024), pp. 79-91. [10.1080/15376494.2023.2245825]

Availability:

This version is available at: 11583/2985073 since: 2024-01-15T10:28:26Z

Publisher:

Taylor and Francis Ltd.

Published

DOI:10.1080/15376494.2023.2245825

Terms of use:

This article is made available under terms and conditions as specified in the corresponding bibliographic description in the repository

Publisher copyright

(Article begins on next page)

A regularized higher-order beam elements for damage analysis of reinforced concrete beams

J. Shen, M. R. T Arruda, A. Pagani & E. Carrera

To cite this article: J. Shen, M. R. T Arruda, A. Pagani & E. Carrera (2024) A regularized higher-order beam elements for damage analysis of reinforced concrete beams, *Mechanics of Advanced Materials and Structures*, 31:1, 79-91, DOI: [10.1080/15376494.2023.2245825](https://doi.org/10.1080/15376494.2023.2245825)

To link to this article: <https://doi.org/10.1080/15376494.2023.2245825>



© 2023 The Author(s). Published with license by Taylor & Francis Group, LLC



Published online: 22 Aug 2023.



Submit your article to this journal [↗](#)



Article views: 387



View related articles [↗](#)



View Crossmark data [↗](#)



Citing articles: 3 View citing articles [↗](#)

ORIGINAL ARTICLE



A regularized higher-order beam elements for damage analysis of reinforced concrete beams

J. Shen^a, M. R. T Arruda^b, A. Pagani^a , and E. Carrera^a

^aMul² Team, Department of Mechanical and Aerospace Engineering, Politecnico di Torino, Torino, Italy; ^bCERIS, Instituto Superior Técnico, Universidade de Lisboa, Lisbon, Portugal

ABSTRACT

This work presents a numerical method for damage analysis of reinforced concrete beams using the higher-order beam theory based on Carrera unified formulation. The component-wise approach is employed to model the concrete and steel reinforcing bars as two independent one-dimensional finite elements. A modified Mazars damage model with tensile and compressive damage propagation laws is utilized for concrete, and an elastic-perfectly plastic law is used for steel rebars. To address the instability and mesh dependence caused by the strain-softening behavior of concrete, a fracture energy regularization technique based on the crack band model is developed, especially for the higher-order beam theory. The proposed method is validated by comparing its numerical results with three experimental benchmark results. The comparison indicates that the method accurately predicts the damage distribution of concrete and the flexural behavior of RC beams under quasi-static loading conditions while remaining computationally efficient.

ARTICLE HISTORY

Received 6 June 2023
Accepted 4 August 2023

KEYWORDS

Reinforced concrete; fracture energy regularization; Mazars damage model; Carrera unified formulation; finite element method

1. Introduction



Reinforced concrete (RC) structures, which consist of concrete and steel, are widely employed in civil engineering. Many researchers utilized computational techniques such as the finite element method (FEM) for structural analysis and design instead of experimental campaigns. However, the elastic-plastic behavior of steel and the quasi-brittle nature of concrete poses challenges for non-linear numerical analysis of RC structures. Moreover, the accurate simulation of crack initiation and propagation is crucial in capturing the behavior of concrete. In RC structures, cracks may develop not only externally but also at the interfaces between steel rebars and the surrounding concrete, thereby adding complexity to the fracture analysis of RC structures.

The simulation of crack formation and growth in RC structures is crucial for evaluating their structural performance. Two commonly employed approaches to simulate the non-linear behavior of pure concrete structures or RC structures are the discrete model [1, 2] and the continuum damage model [3, 4]. The discrete crack model allows displacement discontinuity by introducing interface elements to all element boundaries. However, the model depends on the mesh boundaries, and a re-meshing technique is required, leading to highly refined meshes [5]. Consequently, the concept of strong discontinuity [6] has been developed to capture the arbitrary cracks in concrete,

further contributing to the development of extended FEM (XFEM) [7, 8], embedded FEM (EFEM) [9, 10], and other related methods.

Alternatively, the continuum damage model is more popular due to its computational convenience. In this approach, concrete is treated as a continuum media, and the degradation of concrete stiffness represents the discontinuity caused by cracks. This method is easily combined with the analysis of rebars since physical discontinuous field deformation is explicitly required [11, 12]. Currently, the plastic deformation of steel can be simulated accurately through the FEM with Von Mises plasticity model [13]. Several popular continuum damage models have been proposed and validated, including isotropic [14] and anisotropic damage models [15]. For complex loadings, damage-plasticity models [16, 17] have been proposed to consider both the inelastic and damage-dependent behavior of the material.

One issue associated with the continuum damage model is the occurrence of energy dissipation in localized regions rather than distributed zones when concrete strain softening occurs [18]. This phenomenon can lead to the pathological sensitivity of the numerical results to the element characteristics. Various localization limiters have been proposed to mitigate the mesh-dependency issue, such as nonlocal models, including integral [19] and gradient models [20], where stress at a point depends on the strain at both the local and neighboring points. Another simpler limiter is the crack

CONTACT A. Pagani  alfonso.pagani@polito.it  Mul² Team, Department of Mechanical and Aerospace Engineering, Politecnico di Torino, Corso Duca degli Abruzzi 24, 10129 Torino, Italy.

© 2023 The Author(s). Published with license by Taylor & Francis Group, LLC

This is an Open Access article distributed under the terms of the Creative Commons Attribution License (<http://creativecommons.org/licenses/by/4.0/>), which permits unrestricted use, distribution, and reproduction in any medium, provided the original work is properly cited. The terms on which this article has been published allow the posting of the Accepted Manuscript in a repository by the author(s) or with their consent.

band model [21], which helps to restore the objectivity of numerical solutions by adjusting the concrete constitutive laws. This method introduces a characteristic element length to rescale the post-peak part of the concrete stress-strain law to avoid the tendency of fracture energy to approach zero. However, the correct way to determine the characteristic length for a given finite element remains an open question [22].

While traditional 1-dimensional (1D) models like the Euler-Bernoulli Beam Model (EBBM) and Timoshenko Beam Model (TBM) help capture the bending behavior of simple, slender structural members, their low computational costs are insufficient for capturing the material non-linearity due to cracking in RC heterogeneous structures. For detailed and accurate analysis of such structures, 3-dimensional (3D) models are required. Various 3D models have been developed in which 3D solid finite elements are adopted for concrete and beam or truss elements are employed for rebars [11, 23, 24]. Interface models have also been added to account for bond-slip between concrete and reinforcing bars [25, 26]. However, the computational costs associated with these models are heavy, particularly for large-scale structures. Homogenization techniques [27, 28] can be utilized to combine the behavior of concrete and steel to address these cost issues.

To balance the computational efficiency of 1D models and the elaboration of 3D models, a higher-order beam theory [29] based on Carrera Unified Formulation (CUF) [30] can be employed. According to CUF, a higher-order 1D beam model is utilized, and 3D displacement fields can be obtained by expanding the cross-section using various polynomials, such as Taylor [31] and Lagrange [32]. In the framework of CUF, the orders of the approximation function for the beam element and the expanded function for the cross-section are considered as the input of analysis, eliminating the need for ad hoc assumptions. Lagrange expansion is preferred because it enables CUF to handle arbitrary geometries for both static and free-vibration analyses [33, 34]. Another developed method for analyzing composite structures with two or more parts, such as fiber-reinforced structures, is the Component-Wise (CW) approach based on CUF [35]. This approach divides the structures into different components based on the materials used, and each component can be modeled individually and simultaneously using Lagrange expansion cross-sectional elements. [36] has demonstrated the superior performance of the CW approach compared to other modeling approaches based on CUF, although only linear static analysis was conducted. Moreover, [37] has presented a damage analysis of notched RC beams based on 1D-CUF models under direct tension, which is not a typical loading condition in real engineering applications.

In this context, this study aims to develop a method for simulating the non-linear behavior of bend-dominated reinforced concrete (RC) structures using 1D-CUF models that accurately predict experimental results. To accomplish this, we combine a modified Mazars damage model, which is effective in pure concrete damage modeling [38, 39], with

the plastic behavior of steel rebars. To model cracks at the interface, we approximate them by locally initiating and evolving concrete damage around the steel rebars, avoiding the need for interface models. Additionally, we address the mesh dependence caused by concrete strain-softening by adopting a fracture energy regularization technique based on the crack band model and designing a consistent characteristic element length specifically for 1D-CUF models. Overall, the novelty of this work lies in developing an advanced numerical model based on a simple damage model for non-linear analysis of RC structures, which can be easily implemented in actual engineering design.

This paper is organized as follows: First, some methodologies, including 1D higher-order beam theory, the CW approach, and a modified Mazars damage model, are presented. Next, three bending-dominated RC beams are simulated and compared with corresponding experimental results. Finally, some meaningful conclusions are drawn from the previous analysis.

2. Unified higher-order beam theory

The present work is based on a one-dimensional beam model derived from CUF and implemented using FEM [30]. In the framework of CUF, 3D displacement of the 1D beam model can be enriched by expanding the corresponding cross-section, which is expressed as:

$$\mathbf{u}(x, y, z) = F_\tau(x, z)\mathbf{u}_\tau(y), \quad \tau = 1, 2, \dots, M \quad (1)$$

where $\mathbf{u}_\tau(y)$ represents the generalized displacement vector of beam model; F_τ is the expansion function related to cross-section; τ is an Einstein notation indicating summation and M is the number of terms in the expansion function.

This work adopts Lagrange-type expansion (LE) for F_τ as it can handle any arbitrary cross-section. Quadrilateral elements such as four-node linear (L4), nine-node quadratic (L9), and sixteen-node cubic (L16) are typically used due to their higher accuracy. More detailed information on LE can be found in [30].

By discretizing the beam using the classical finite element method, the displacement field can be rewritten as:

$$\mathbf{u}(x, y, z) = F_\tau(x, z)N_i(y)\mathbf{u}_{ti}, \quad i = 1, \dots, N_{NE} \quad (2)$$

where \mathbf{u}_{ti} is the nodal displacement vector, and N_i is the beam shape function with N_{NE} nodes per beam element.

Typically, two-node linear (B2), three-node quadratic (B3), and four-node cubic (B4) beam elements are commonly used. The detailed shape functions for these elements can also be found in [30]. However, it is essential to note that the choice of beam finite elements is independent of the selection of the class and order of the expansion function, which is one of the advantages of CUF models.

The governing equation for static problems can be obtained using the principle of virtual displacements. The detailed derivation process can be found in [39]. For the sake of simplicity, the final equation is provided below:

$$\mathbf{K}^{\tau sj} \mathbf{u}_{ti} = \mathbf{F}_{sj} \quad (3)$$

where F_{sj} is the nodal external force vector, and K^{tsij} is the fundamental nucleus of the stiffness matrix, which can be computed as:

$$K^{tsij} = \int_l \int_{\Omega} D^T [N_j(y) F_s(x, z)] C D [F_t(x, z) N_i(y)] d\Omega dl \quad (4)$$

where l and Ω represent the length of beam element and area of cross-section, respectively; C is the material matrix; D is the differentiation operator; i, j , and τ, s are indexes related to beam shape function and cross-sectional expansion function respectively. The integral in Equation 4 is obtained numerically using the Gauss quadrature technique, which is given explicitly in [30].

3. Component-wise approach

The reinforced concrete beam is a kind of composite structure that is made of steel and concrete (Figure 1a). An extension of 1D-CUF models, known as the component-wise approach, is utilized to model the concrete and steel individually and simultaneously. As shown in Figure 1b, the steel rebars and surrounding concrete are considered independent components using the same beam elements. The cross-section can then be discretized into multiple Lagrange elements with different materials, and the Lagrange points in the boundaries of other materials can ensure the continuity conditions among the various components, as shown in Figure 1c.

Through this approach, the CUF model allows each component to maintain its independent material and geometrical properties. A refined model can also be determined for the interested component as needed. Some examples of the CW approach can be found in [36, 37].

4. Modified Mazars damage model

This section discusses a modified Mazars damage model with fracture energy regularization technique to obtain the objectivity of RC damage analysis. Mazars damage model is an isotropic damage model for concrete described in [14]. This model is based on the theory of elasticity coupled with damage mechanics. It employs a scalar damage variable to account for the uniform degradation of the stiffness properties in all directions. This variable depends only on the positive effective strains in the principle directions.

Compared to other damage models, such as concrete damage plasticity (CDP), the Mazars damage model does not consider permanent strains. However, it is adequate for damage analysis of RC structures under quasi-static load because the plastic behavior from rebars plays a more critical role in RC structures. Besides, when using fracture energy regularization for tension and compression, the structural response can get regularized and no longer be mesh dependent. Moreover, introducing this regularization can eliminate the need for fitting parameters. Therefore, the proposed model is ideal for practical structural design due to its simplicity and robustness.

4.1. Model formulation

Mazars [14] introduced a scalar variable for classical Hooke's law to consider the non-linear behavior of concrete material, which is written as:

$$\sigma = (1 - d) C \varepsilon \quad (5)$$

where σ and ε represent the stress and strain vector; d is the damage variable used to monitor the stiffness degradation.

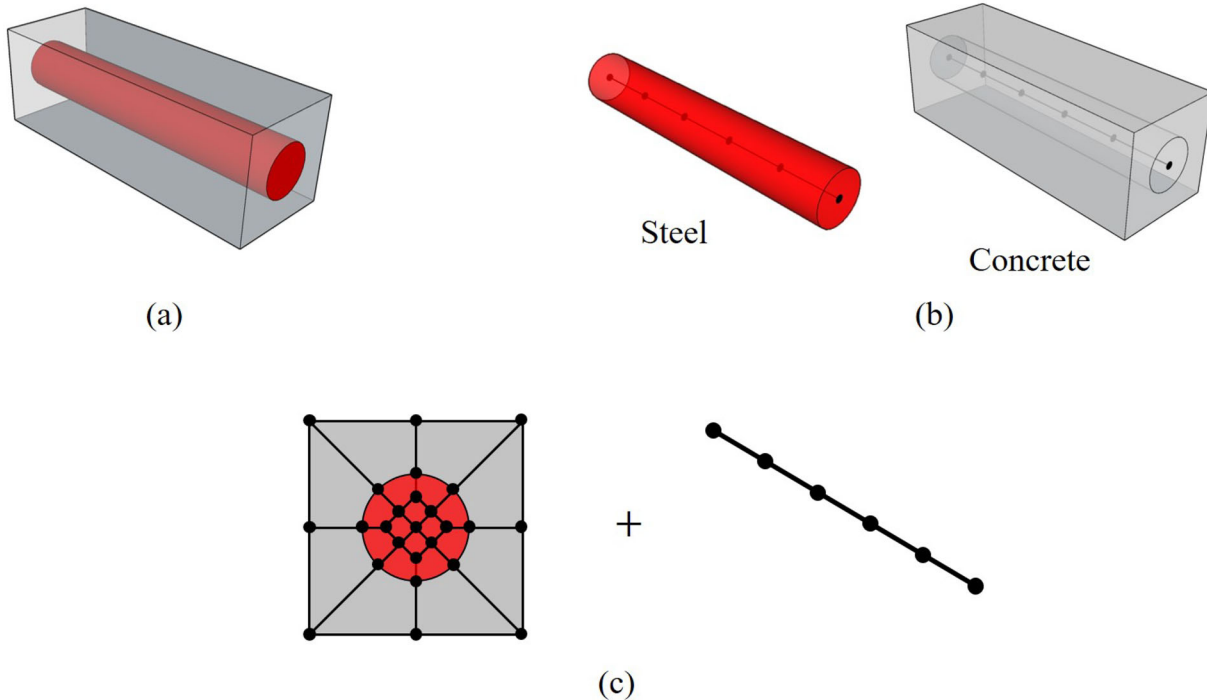


Figure 1. An illustration of CW approach for modeling RC structures: a) definition of RC structures, b) individual steel and concrete component, and c) assembled cross-section with Lagrange elements along with the beam.

The positive principle strain governs the initiation of both tensile and compressive damage. Therefore, an equivalent strain ε_{eq} , as defined by Mazars, is calculated as:

$$\varepsilon_{eq}(\boldsymbol{\varepsilon}) = \sqrt{\sum_{i=1}^3 \langle \varepsilon_i \rangle_+^2} \quad (6)$$

where $\langle \cdot \rangle_+$ is the Macauley bracket for picking out the positive value, and ε_i are the principle strains. Then the loading function is:

$$f(\boldsymbol{\varepsilon}, \kappa) = \varepsilon_{eq}(\boldsymbol{\varepsilon}) - \kappa \quad (7)$$

where κ is a threshold of damage growth that equals the ultimate tensile strain of material at first and then keeps updated as the $\varepsilon_{eq}(\boldsymbol{\varepsilon})$ after first damage.

4.2. Damage propagation

Once $f(\boldsymbol{\varepsilon}, \kappa) \geq 0$ in Equation 7, the damage is activated and determined by a combination of tensile and compressive damage responses. This can be expressed as:

$$d = \alpha_t d_t + \alpha_c d_c \quad (8)$$

where α_t and α_c are weights that link the damage variable in tension d_t and compression d_c . The explicit calculation of α_t and α_c can be found in [38].

The damage variables are related to the internal variable κ which equals to the equivalent strain under monotonic loading [22]. While the original Mazars damage model [14] also provided damage propagation laws for d_t and d_c , these require fitting experimental results to obtain some parameters. In this work, modified damage evolution laws for tension and compression are adopted based on concrete constitutive laws (Figure 2) from fib MC2010 [40], which are more practical. Additionally, a fracture energy regularization technique based on crack band model is employed to regularize the softening behavior and prevent mesh dependency.

For simplicity and brevity, the damage evolution law of tension is shown as Eq 9, which is derived from a classical exponential softening constitutive law depicted in Figure 2a.

More detailed information on this derivation can be found [38].

$$d_t = g_t(\kappa_t) = \begin{cases} 1 - \frac{\varepsilon_{d0}}{\kappa_t} \exp\left(\frac{\varepsilon_{d0} - \kappa_t}{\varepsilon_{tu} - \varepsilon_{d0}}\right) & \text{if } \kappa_t \leq \varepsilon_{tres} \\ 1 - \frac{p_t \times \varepsilon_{d0}}{\kappa_t} & \text{if } \kappa_t > \varepsilon_{tres} \end{cases} \quad (9)$$

where ε_{d0} is the limit elastic strain, which is calculated by dividing the mean uniaxial tensile strength f_{ctm} by Young's modulus E ; p_t is residual tensile stress ratio that is the ratio between the residual tensile stress and f_{ctm} , which ensures the value of damage not equal 1.0 but infinitely close to 1.0; ε_{tres} is the corresponding residual tensile strain; ε_{tu} is the equivalent ultimate strain for bilinear softening, which is shown in Figure 2a and calculated as:

$$\frac{G_{ft}}{l_c} = f_{ctm}(\varepsilon_{tu} - \varepsilon_{d0}) \quad (10)$$

where G_{ft} is the fracture energy of mode I cracking. ε_{tu} can be adjusted to control the slope of the softening diagram through introducing the characteristic element length l_c .

Similarly, the damage evolution law of compression is derived from compressive stress-strain curve depicted in Figure 2b and the explicit formulation is expressed as:

$$d_c = g_c(\kappa_c) = \begin{cases} 1 - \frac{(k \times \bar{\varepsilon}_c - \bar{\varepsilon}_c^2) f_{cm}}{(1 + (k-2) \times \bar{\varepsilon}_c) E_{cm} \kappa_c} & \text{if } \kappa_c \leq \varepsilon_{c1} \\ 1 - \frac{f_{cm}}{E_{cm} \kappa_c} & \text{if } \varepsilon_{c1} < \kappa_c \leq \varepsilon_{c2} \\ 1 + \frac{k_1}{E_{cm}} - \frac{k_2}{E_{cm} \kappa_c} & \text{if } \varepsilon_{c2} < \kappa_c \leq \varepsilon_{cres} \\ 1 - \frac{p_c f_{cm}}{E_{cm} \kappa_c} & \text{if } \varepsilon_{cres} < \kappa_c \end{cases} \quad (11)$$

with

$$\begin{aligned} \kappa_c &= \frac{\kappa_t}{\nu\sqrt{2}}; \quad \bar{\varepsilon}_c = \frac{\kappa_c}{\varepsilon_{c1}}; \quad k = \frac{1.05 E_{cm} \varepsilon_{c1}}{f_{cm}}; \quad k_1 \\ &= \frac{f_{cm}}{(\varepsilon_{cu} - \varepsilon_{c2})}; \quad k_2 = f_{cm} + k_1 \times \varepsilon_{c2}; \end{aligned}$$

where f_{cm} is the mean compressive strength of the concrete;

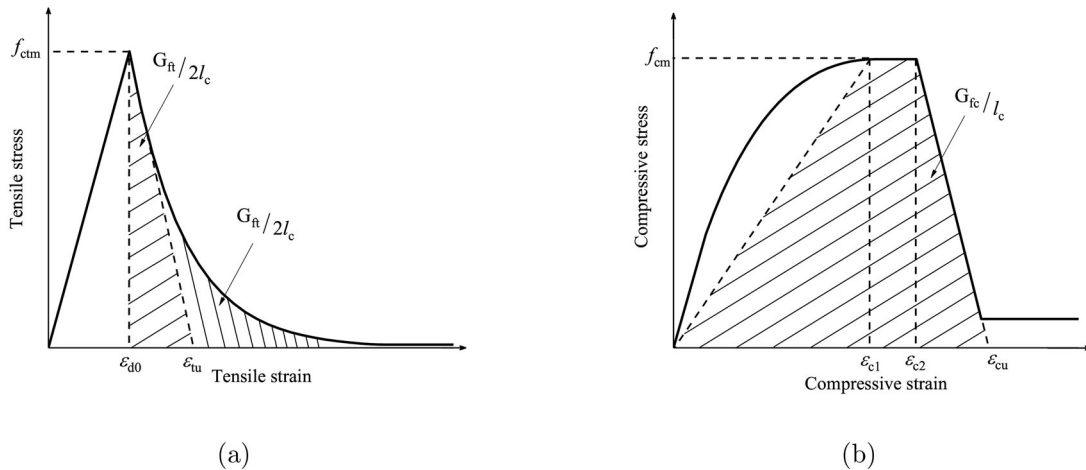


Figure 2. Concrete constitutive laws for modified Mazars damage model: a) tension and b) compression.

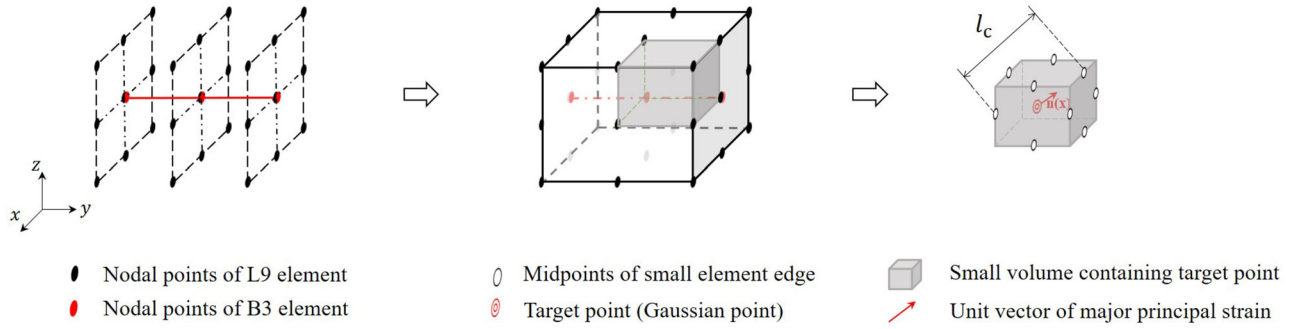


Figure 3. An illustration of estimation method for l_c .

E_{cm} is the secant Young's modulus; k , k_1 and k_2 are parameters from [41] to describe the softening part of constitutive laws; ε_{c1} and ε_{c2} are strain parameters adopted from [41], respectively; $\bar{\varepsilon}_c$ is a unidimensional strain ratio provided in [40]. p_c is residual compressive stress ratio that is the ratio between the residual compressive stress and f_{cm} , which ensures stress never equals 0.0 to avoid convergence problem; ε_{cres} is the corresponding residual compressive strain; ε_{cu} is the extreme compressive strain, which is shown in Figure 2b and calculated by:

$$\frac{G_{fc}}{l_c} = f_{cm} \times \left(\frac{\varepsilon_{cu} + (\varepsilon_{c2} - \varepsilon_{c1})}{2} \right) \quad (12)$$

where G_{fc} represents the energy dissipation per unit area due to crushing. Similarly, the slope of softening part can be controlled by adjusting ε_{cu} through introducing the characteristic element length l_c .

4.3. Characteristic element length

The characteristic element length l_c depends on various aspects of mesh discretization such as element shapes, dimensions, interpolation functions, and so on [22]. In the past, three main methods have been developed to estimate this length: (1) the method based on element area or volume [42], (2) the projection method [43], and (3) Oliver's method [44] which was extended to 3D linear elements by Govindjee [45]. These methods are partially reviewed in [22]. Recently, some modifications [46, 47] have been made to Govindjee's method to improve the accuracy of l_c estimation. However, these methods are limited to linear elements or only validated in 2D problems, making them unsuitable for higher-order beam elements based on CUF.

Given the aforementioned summary, this work employs a new method for estimating the characteristic element length, inspired by [47]. The new estimation method is extensively discussed in [48]. A simple example is employed here for illustration in Figure 3. One B3 element with three nodes is used to model the beam, while one L9 element with nine nodes is used for cross-section expansion. Then, A volume is assembled, as shown in the first two steps of Figure 3. According to the order of beam element and expansion element, the assembled volume is divided into eight small volumes in this case, each containing eight nodes similar to a linear solid element. Next, the middle points of each edge

and the unit vector of the major principal strain at the target point are obtained and stored, assuming that the small gray shaded volume contains an interested point (Gaussian point). Finally, the projection method of [47] is conducted, as shown in the last step of Figure 3, and can be expressed as:

$$l_c(\mathbf{x}) = |l_{\max} - l_{\min}| \quad (13)$$

with

$$\begin{aligned} l_{\max} &= \max[\mathbf{x}_M \cdot \mathbf{n}(\mathbf{x})] \\ l_{\min} &= \min[\mathbf{x}_M \cdot \mathbf{n}(\mathbf{x})] \end{aligned} \quad (14)$$

where \mathbf{x} represents coordinates of the target point; \mathbf{x}_M means all coordinates of middle points from a small volume that containing the target point and $\mathbf{n}(\mathbf{x})$ is the unit vector of principal strain on the target point.

5. Numerical results

In this section, three experimental benchmarks are selected to assess the efficiency and accuracy of proposed method. One benchmark consists of an RC beam with only bottom rebars, while the other two consist of RC beams with stirrups for anti-shear failure. Quasi-static modeling is adopted for all numerical models through displacement-control method.

5.1. Leonhardt shear beam

The first experimental benchmark, named as Leonhardt shear beam, is adopted from [49] to assess the proposed method. This beam is a reinforced concrete beam with a single bottom reinforcement, and its geometric information and boundary conditions are shown in Figure 4. The beam has two longitudinal rebars with a diameter of 26 mm, and the concrete cover is 37 mm. The loading process is displacement-controlled, with a maximum displacement value of 5 mm. The relevant material properties are listed in Table 1. The hardening behavior of the steel rebar is assumed to be perfectly plastic.

The half model, shown in Figure 5a is adopted in finite element analysis as the beam is symmetric across the y axes. The mesh discretizations on cross-section are shown in Figure 5b where there are three different sections, and the steel components are highlighted in red.

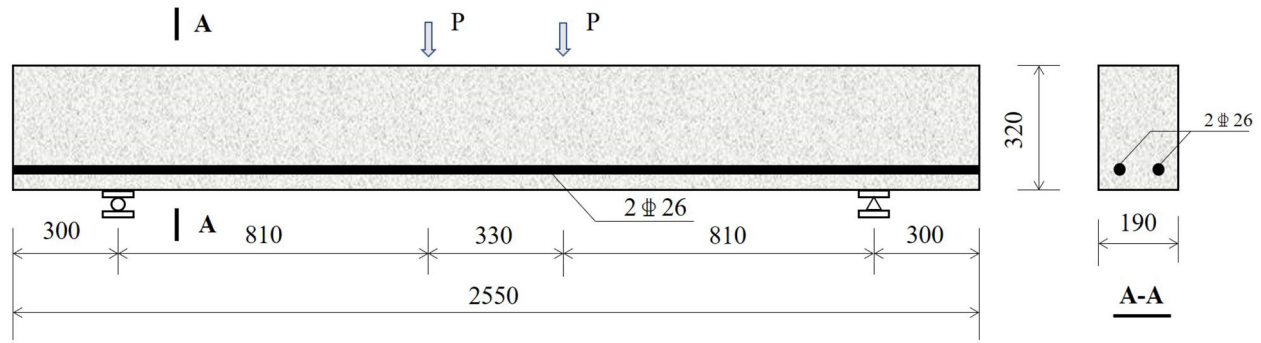


Figure 4. Leonhardt shear beam: geometry and boundary conditions (Unit:mm).

Table 1. Leonhardt shear beam: Material properties.

Material type	E (GPa)	f_{ctm} (MPa)	f_{cm} (MPa)	G_R (N/m)	G_{fc} (N/m)	ν	f_y (MPa)
Concrete	31.72	1.64	28.48	100.0	19870	0.2	–
Steel	208	–	–	–	–	0.3	560

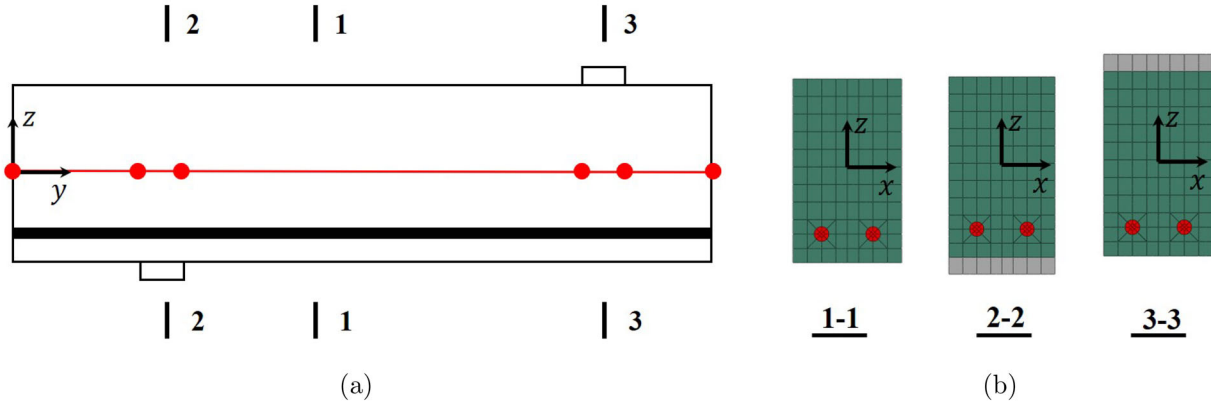


Figure 5. Mesh assignment of Leonhardt beam: (a) Beam element; (b) LE cross-section discretization.

Table 2. Leonhardt shear beam: mesh configurations.

Model No.	Model A	Model B	Model C	Model D
Beam element	20B4	20B2	20B2	34B2
LE	L9	L9	L4	L4
DoFs	96885	33789	9078	14958

Table 2 lists four models used to study the mesh-independence of the proposed method. The discretizations of cross-sections are the same for all models, while Model C and D adopt linear elements and Models A and B use quadratic elements. Model A adopts higher-order beam elements with higher-order cross-section expansion, which should provide the highest accuracy due to highest number of degrees of freedom (DoFs). Compared to Model A, Model B and Model C investigate saving the computational costs by reducing the order of beam elements and cross-section expansion, respectively. Model D investigates convergence and mesh-independence by increasing the number of beam elements compared to Model C.

Figure 6 plots the displacement at the center of the beam versus the reaction force at one of the supports from four different models, including experimental one for comparison. Before the loading achieves around 36% of maximum displacement (1.8mm), all of the numerical curves match well with the experimental curve and are close to each other.

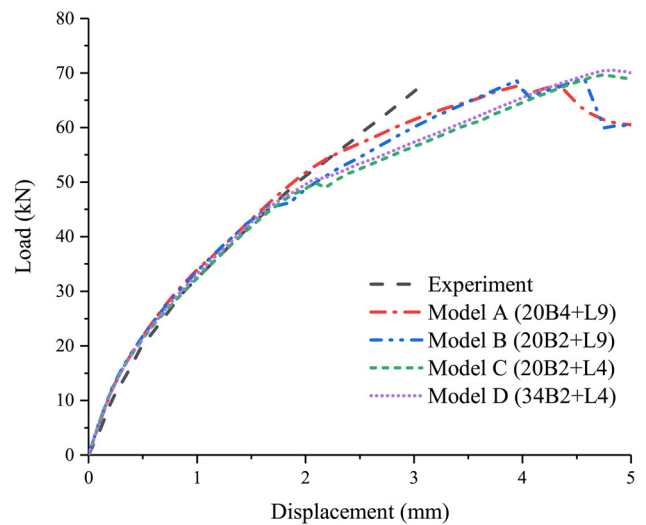


Figure 6. Load-displacement curves of Leonhardt shear beams from different models.

After this point, some small divergence occurs among the different numerical curves, but the stiffness of all numerical models remains similar. The experimental peak load is approximately 68.26kN with a corresponding displacement of approximately 3.1mm. All of the numerical models can achieve the peak value, but the corresponding displacements

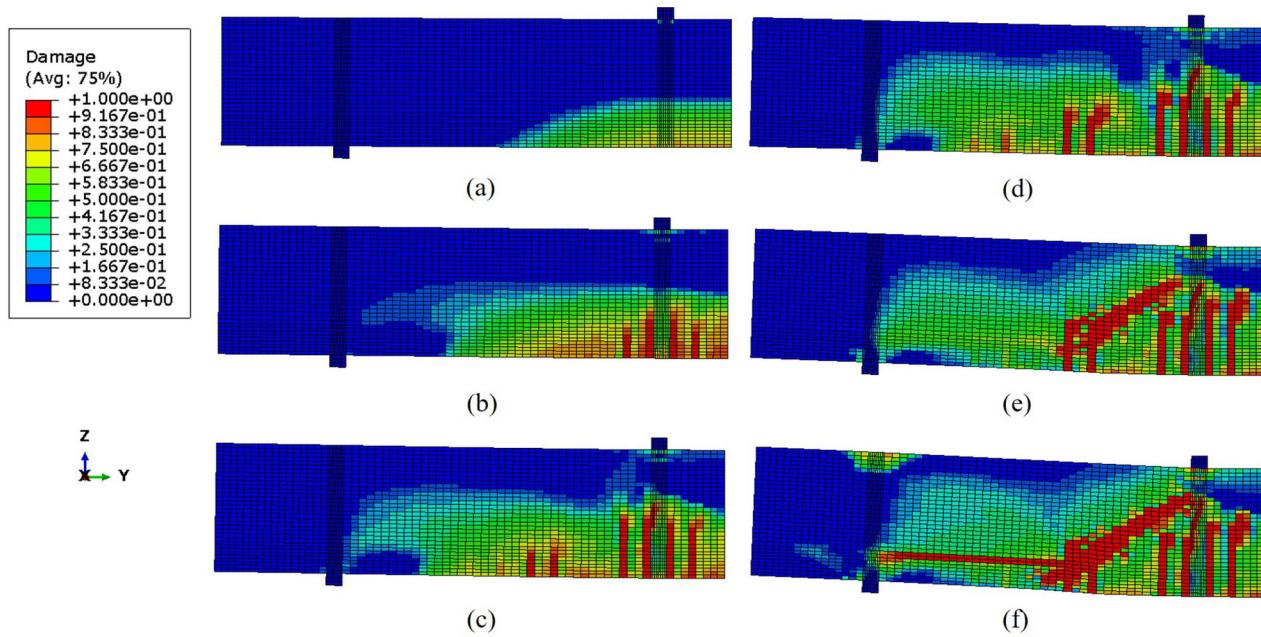


Figure 7. Damage distributions of Model A (20B4 + L9) at: a) 8%, b) 16%, c) 24%, d) 36%, e) 64%, and f) 80% of the maximum displacement.

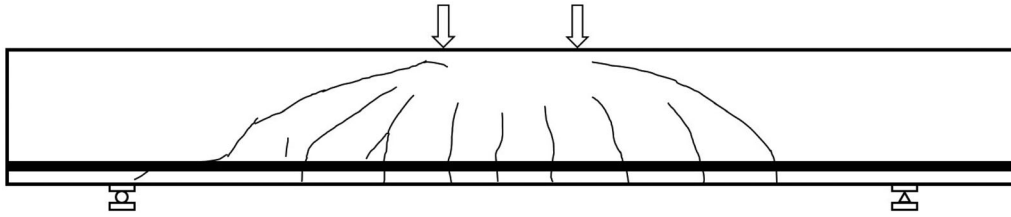


Figure 8. Cracks observed in the experiment of Leonhardt shear beam.

are around 4.5mm . This difference is because the numerical stiffness of the latter part is clearly lower than the experimental stiffness.

To explain the above phenomenon, Figure 7 displays damage propagation during loading. For comparison, observed cracks in the experiment are plotted in Figure 8. Initially, damage occurs at the bottom and propagates vertically from Figure 7a–c due to beam bending. Following this, damage develops obliquely because of shear behavior, as demonstrated from Figure 7d–e. At this stage, the numerical stiffness exhibits a reduction, falling below the experimental value. Finally, horizontal damage is formed, connecting the support and the previously developed diagonal damage, as seen in Figure 7f. The final damage distribution is akin to the actual experimental cracks, except that a diagonal crack connecting the support and loading point was observed from the experimental campaign. However, it is essential to note that the proposed modified Mazars damage model only considers tensile and compressive damage based on fracture mode I and does not consider shear fracture. This drawback can account for the slight discrepancy between the numerical and experimental stiffness in the later stage.

Figure 9 illustrates the damage distributions at a displacement of 4mm for different numerical models to investigate the objectivity of numerical models. It turns out that all models predict a similar damage distribution, with some vertical damage occurring in the mid-span and horizontal

damage connected to one oblique damage in the side span. Combining this with the nonlinear performance shown in Figure 6, it can be concluded that the proposed method can provide mesh-independent results with any mesh configuration, even with Model C, which has less than 10,000 degrees of freedom.

5.2. Four-point bending RC beam

This experimental benchmark was reinforced with stirrups to resist the shear behavior. It was reported in [50, 51] that the concrete collapse occurred due to the failure of concrete compression. Therefore, it is an important benchmark for validating regularized higher-order finite elements associated with compressive fracture energy. The geometric and boundary conditions are reported in Figure 10, with stirrups reinforced every 60mm and a concrete cover thickness of 15mm . The material properties are listed in Table 3. A bilinear model is used for steel initially, followed by an elastic-plastic model after ultimate strain.

Figure 11 illustrates the beam mesh and cross-sectional expansions used for the numerical analysis. A similar half-structure is adopted as in the previous benchmark, but more beam elements are required due to the presence of stirrups, which result in a periodic change of the cross-section.

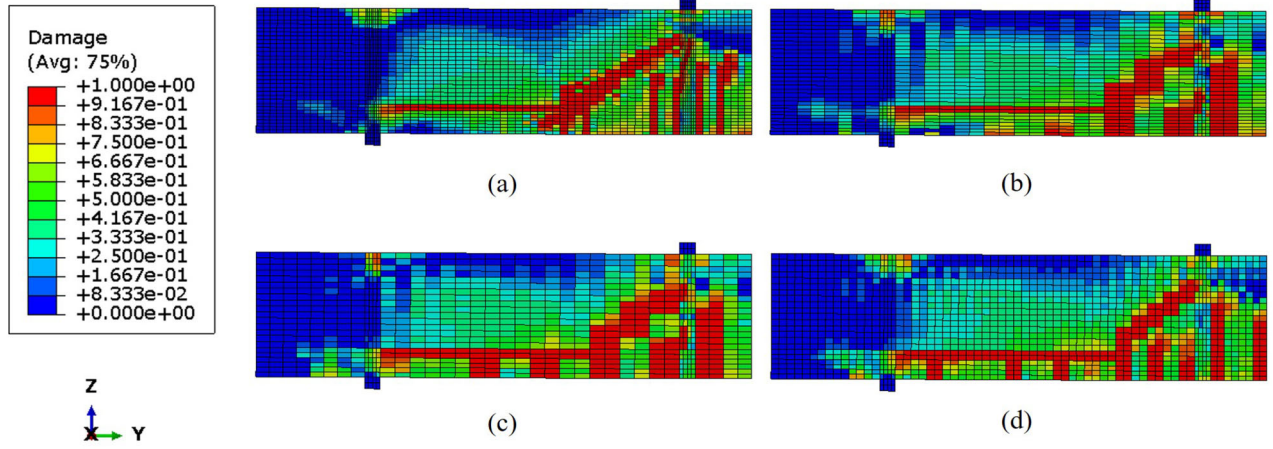


Figure 9. Damage distributions of Leonhardt shear beams at 4 mm from: a) Model A (20B4 + L9); b) Model B (20B2 + L9); c) Model C (20B2 + L4); d) Model D (34B2 + L4).

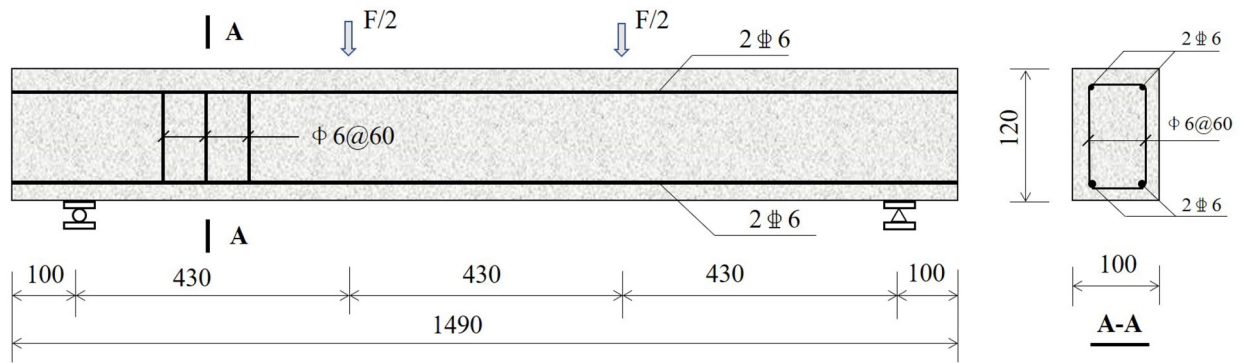


Figure 10. Four-point bending RC beam: geometry and boundary conditions (Unit:mm).

Table 3. Four-point bending RC beam: material properties.

Material	E (GPa)	f_{ctm} (MPa)	f_{cm} (MPa)	G_{ft} (N/m)	G_{fc} (N/m)	ν	f_y (MPa)	f_{yu} (MPa)
Concrete	31.0	2.8	37	140.0	21000	0.2	–	–
Steel	193	–	–	–	–	0.3	546	691

Table 4. Four-point bending RC beams: mesh configuration.

Model No.	Model 1	Model 2	Model 3	Model 4
Beam element	75B2	40B2	40B3	40B4
LE	L9	L9	L9	L9
DoFs	102696	55551	109647	163743

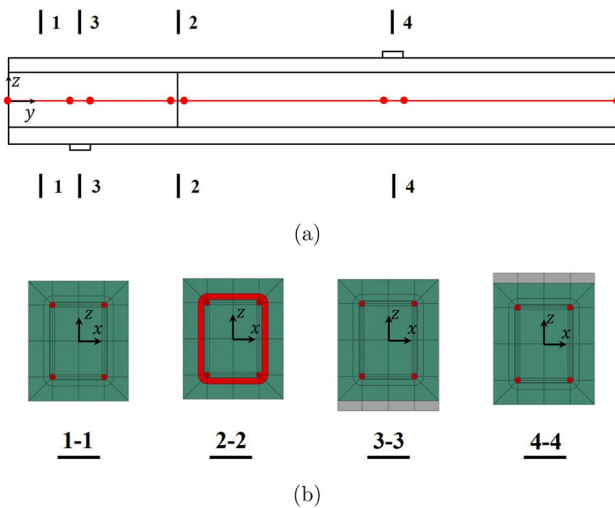


Figure 11. Mesh assignment of four-point bending RC beam: (a) Beam element; (b) LE cross-section discretization.

To investigate the objectivity of numerical results obtained from different mesh configurations, four models listed in Table 4 are designed. The cross-sectional

expansions are kept the same for four models to investigate the influence of the number and order of beam elements.

Figure 12 displays the load-displacement curves for various models, and the experimental curve is included for comparison. The numerical curves exhibit high similarity regardless of the mesh configurations adopted. The initial linear stiffness obtained from the numerical results agrees with the experimental value. However, the crack loads predicted by all the models are higher than the experimental value. This discrepancy is attributed to initial cracks or defects in the experimental specimens, also reported in [38]. Subsequently, the stiffness at the inelastic stage with cracks predicted by the numerical results closely approximates the experimental campaign results. Finally, The numerical curves corresponding to phase III also show a good agreement with the experimental curve. Overall, these results demonstrate the robustness and reliability of the proposed numerical models, with mesh-independent results that accurately capture the material's behavior under both elastic and inelastic phases.

Figure 13 depicts the damage propagation during the loading process, with all diagrams presented considering the deformed shape. Initially, multiple micro-cracks occur at the bottom of the beam, with the corresponding crack load being around 7.15kN , which matches well with the expected value from [38]. As the loading continues, vertical damage propagates, and the steel rebars begin to yield, as shown in Figure 14, at 18% of the maximum displacement. The corresponding damage distribution is shown in Figure 13c. The concrete begins to crush at around 50% of the maximum

displacement, as shown in Figure 13d, with damage also occurring at the top middle part. Last, Figure 13e presents the final vertical damage, which is similar to vertical cracks shown in Figure 15.

5.3. Three-point bending RC beam

The last benchmark is a three-point bending test of a concrete beam reinforced with longitudinal steel bars and stirrups conducted in [52]. The geometric and reinforcement design of the tested specimen is shown in Figure 16. The beam is subjected to a single concentrated vertical load at

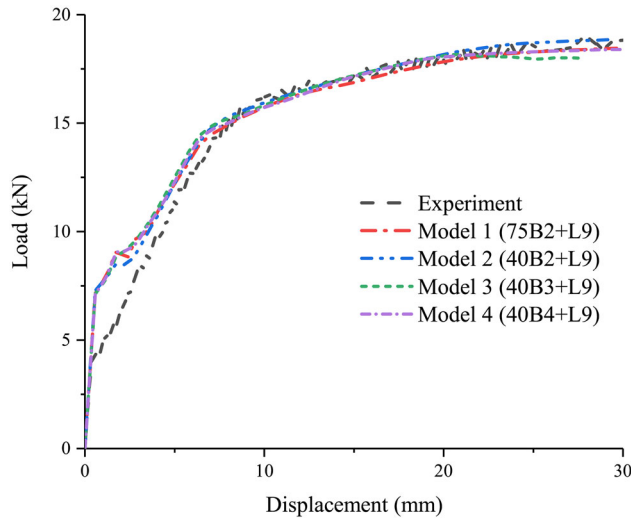


Figure 12. Load-displacement curves of four-point bending RC beams from different models.

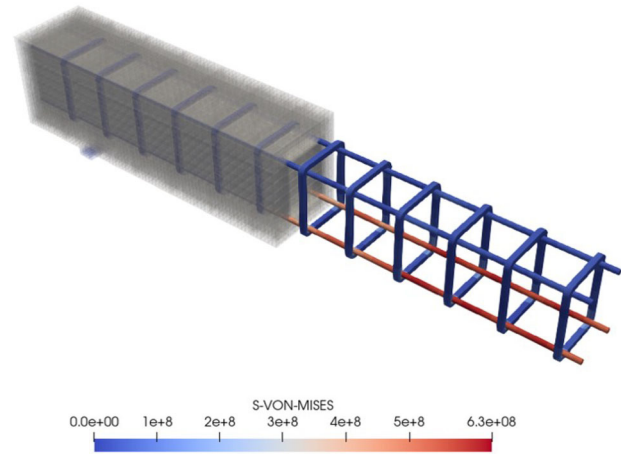


Figure 14. Von Mises stress distribution of steel rebars at 18% of the maximum displacement.

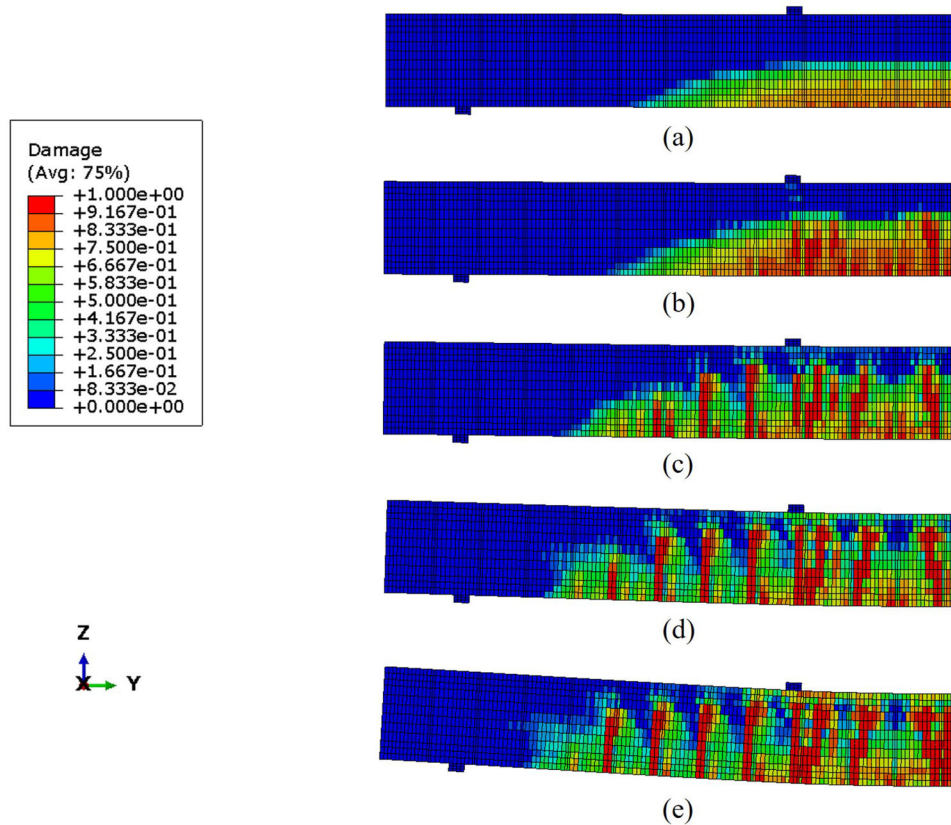


Figure 13. Damage distribution of Model 1 (75B2 + L9) at: a) 2%; b) 6%; c) 18%; d) 50%; e) 100% of the maximum displacement.

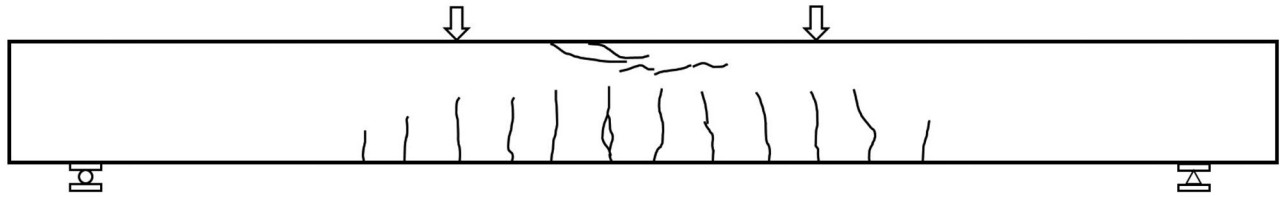


Figure 15. Crack distribution from the experiment of four-point bending RC beam.

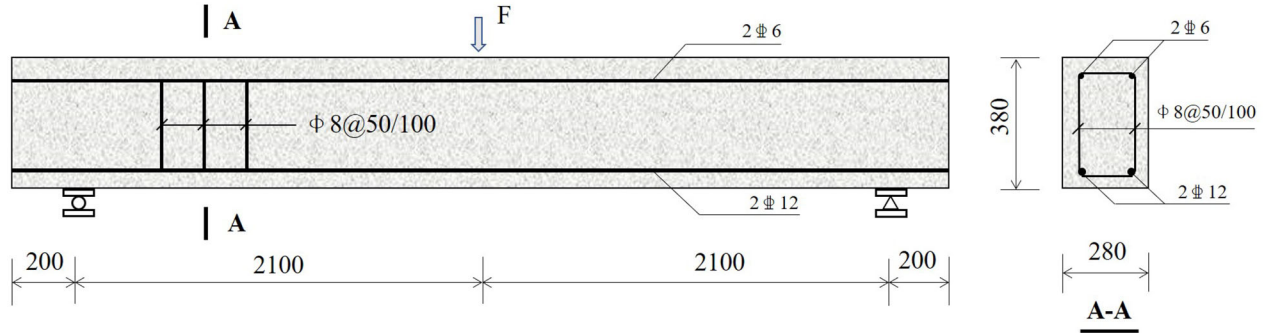


Figure 16. Three-point bending RC beam: geometry and boundary conditions (Unit:mm).

Table 5. Three-point bending RC beam: material properties.

Material type	E (GPa)	f_{ctm} (MPa)	f_{cm} (MPa)	G_R (N/m)	G_{Rc} (N/m)	ν	f_y (MPa)
Concrete	32.12	2.0	35.3	70.0	21000	0.167	–
Steel	220.0	–	–	–	–	0.28	507.0

Table 6. Four-point bending RC beams: mesh configuration.

Model No.	Model I	Model II	Model III
Beam element	59B2	77B2	121B2
LE	L9	L9	L9
DoFs	99198	128844	201312

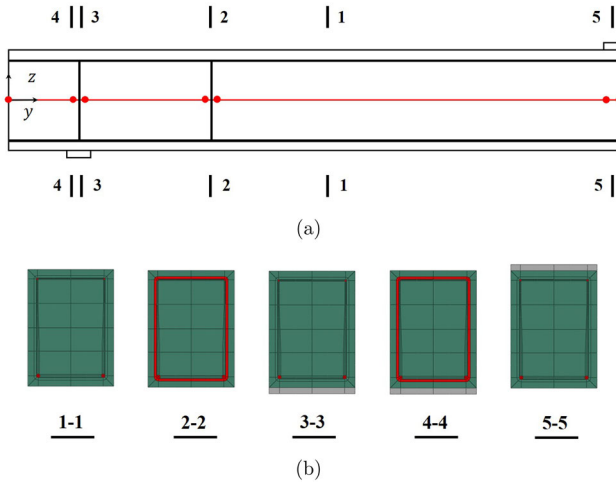


Figure 17. Mesh assignment of three-point bending RC beam: (a) Beam element; (b) LE cross-section discretization.

the top mid-span, with a maximum displacement control of 5 mm. The stirrups are spaced at 100 mm in the span and reduced to 50 mm near both ends (each along 500 mm). Only two longitudinal steel bars are placed at the bottom and top, and the concrete protective thickness is 20 mm. Therefore, the beam was characterized as under-reinforced and failed in ductile flexure, with the yielding of steel rebars followed by concrete crushing, as reported in [52]. The beam is relatively large compared to the previous two benchmarks, making it ideal for validating the proposed method. Material properties of concrete and steel are listed in Table 5.

Similarly to the previous benchmarks, a half structure is adopted due to symmetry across the y axis. The beam element assignment and cross-section discretization are shown in

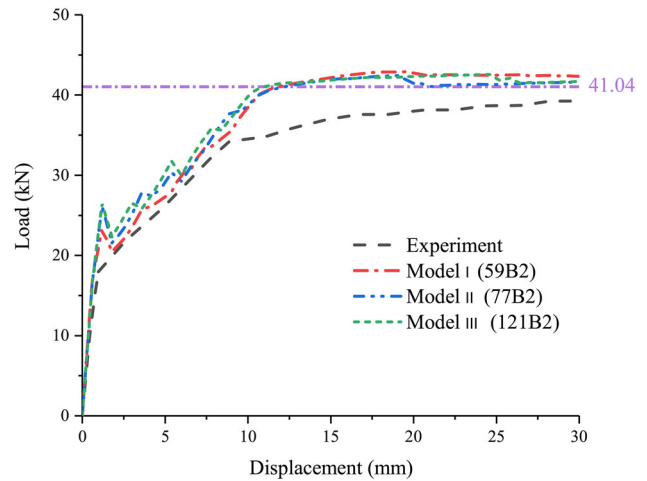


Figure 18. Load-displacement curves of three-point bending RC beams from different models.

Figure 17. Commonly, one beam element should be assigned along the thickness of the stirrups, and another one should be assigned along the space between two adjacent stirrups. Since more stirrups exist in this benchmark, more beam elements are required compared to previous benchmarks.

Due to the large number of stirrups in the structure, a minimum of 59 beam elements are required, as shown in Model I in Table 6. However, finer meshes with more beam elements are also presented, such as Model II and Model III in Table 6. Although only linear beam elements are used, the DoFs are still heavy. Therefore, higher-order elements are not investigated in this case.

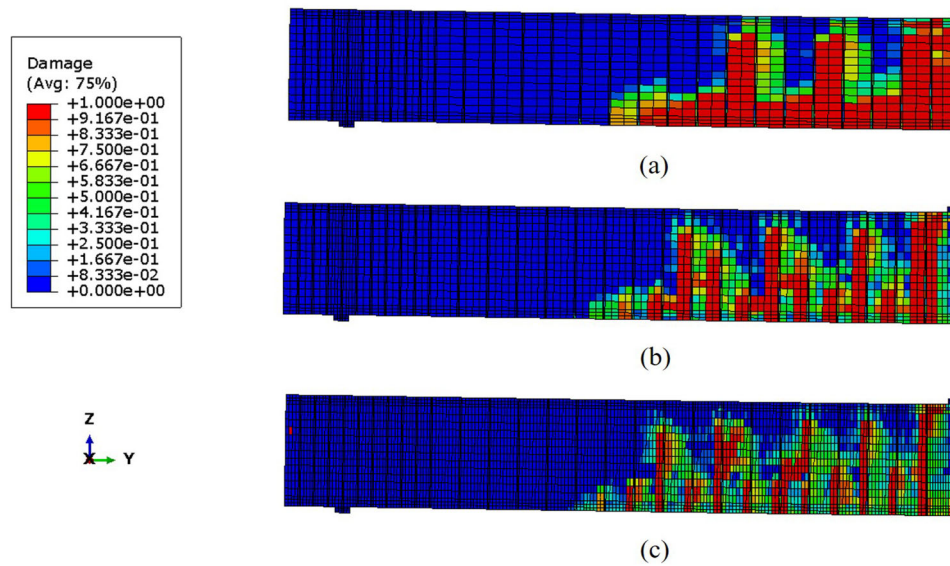


Figure 19. Final damage distribution of: a) Model I, b) Model II, and c) Model III.

Figure 18 compares the load-displacement curves obtained from the three numerical models and the experimental result. The curves from the numerical models exhibit a high degree of similarity, providing evidence for the mesh independence of the proposed method. All numerical models capture the stiffness related to phase I and II well. However, the maximum loads obtained from all numerical models during phase II are slightly higher than the experimental value. The RC beam exhibited its weakest plane at the midspan in the experimental campaign. A stiff plate is added to the top of the FEM model to avoid stress concentration, which leads to the shift of the weakest plane away from the midspan, as shown in Figure 19. Additionally, a higher theoretical ultimate load of around 41.04kN, displayed in Figure 18, is expected if the weakest plane is assumed to occur 200 mm from the midspan. Therefore, the slight discrepancy between experimental and numerical results in the third phase is acceptable.

Figure 19 shows that the finer mesh can provide more detailed and accurate damage distributions compared to the coarser meshes. However, the overall damage patterns, such as the vertical damage caused by bending behavior, are similar for all numerical models.

6. Conclusions

This research work investigated the damage analysis of RC beams using 1D higher-order beam theory based on Carrera unified formulation. The proposed method utilized a component-wise approach to explicitly model the concrete and steel components. The modified Mazars damage model was adopted to evaluate concrete damage, while an elastic-perfectly plastic material response was employed for steel rebars. A fracture energy regularization technique was adopted with a new estimation method for the characteristic element length to mitigate the mesh dependence of finite

element models. The following conclusions were drawn based on the comparisons between numerical and experimental results from three benchmarks of bending-dominated RC beams:

1. In terms of load-displacement curves, the proposed 1D CUF model with the proposed material models can accurately predict both linear and non-linear behavior of RC beams under bending
2. Despite the lack of consideration for mode II shear fracture, the modified Mazars damage model can still capture the similar non-linear behavior of RC shear beams compared to experimental campaigns.
3. The fracture energy regularization technique, with the new estimation method for the characteristic element length, effectively mitigates mesh dependence, allowing for computational costs to be saved by adopting coarser meshes.

Although accurate and robust results were obtained through the proposed model, a large number of DoFs was required if many stirrups were imposed, as seen in the third numerical example, which caused an increase in computational costs. Therefore, ongoing studies will explore adopting a node-dependent kinematic approach [53] to address this issue.

Funding

This research has received funding from the European Research Council (ERC) under the European Union's Horizon 2020 research and innovation programme (Grant agreement No. 850437). Besides, This work has been partly supported by Fundação para a Ciência e Tecnologia, under the Transitional Standard – DL57/2016/N3/UI/CERIS/CT/165/2018.

ORCID

A. Pagani  <http://orcid.org/0000-0001-9074-2558>

References

- [1] A.R. Ingraffea, and V. Saouma, Numerical modeling of discrete crack propagation in reinforced and plain concrete, in *Fracture Mechanics of Concrete: Structural Application and Numerical Calculation*, edited by G.C. Sih, and A. DiTommaso, Springer, Dordrecht, Netherlands, 1985, pp. 171–225, Chapter 4.
- [2] M.V.K.V. Prasad, and C.S. Krishnamoorthy, Computational model for discrete crack growth in plain and reinforced concrete, *Comput. Methods Appl. Mech. Eng.*, vol. 191, no. 25–26, pp. 2699–2725, 2002. DOI: [10.1016/S0045-7825\(02\)00210-4](https://doi.org/10.1016/S0045-7825(02)00210-4).
- [3] J.L. Chaboche, Continuum damage mechanics: part i—general concepts, *Trans. ASME, J. Appl. Mech.*, vol. 55, no. 1, pp. 59–64, 1988. DOI: [10.1115/1.3173661](https://doi.org/10.1115/1.3173661).
- [4] L. Kachanov, *Introduction to Continuum Damage Mechanics*, Springer Science & Business Media, Netherlands, 1986.
- [5] Z.J. Yang, and J.F. Chen, Finite element modelling of multiple cohesive discrete crack propagation in reinforced concrete beams, *Eng. Fract. Mech.*, vol. 72, no. 14, pp. 2280–2297, 2005. DOI: [10.1016/j.engfracmech.2005.02.004](https://doi.org/10.1016/j.engfracmech.2005.02.004).
- [6] J. Oliver, M. Cervera, and O. Manzoli, Strong discontinuities and continuum plasticity models: the strong discontinuity approach, *Int. J. Plast.*, vol. 15, no. 3, pp. 319–351, 1999. DOI: [10.1016/S0749-6419\(98\)00073-4](https://doi.org/10.1016/S0749-6419(98)00073-4).
- [7] A. Yazid, N. Abdelkader, and H. Abdelmadjid, A state-of-the-art review of the x-fem for computational fracture mechanics, *Appl. Math. Modell.*, vol. 33, no. 12, pp. 4269–4282, 2009. DOI: [10.1016/j.apm.2009.02.010](https://doi.org/10.1016/j.apm.2009.02.010).
- [8] A. Faron, and G.A. Rombach, Simulation of crack growth in reinforced concrete beams using extended finite element method, *Eng. Fail. Anal.*, vol. 116, pp. 104698, 2020. DOI: [10.1016/j.engfailanal.2020.104698](https://doi.org/10.1016/j.engfailanal.2020.104698).
- [9] J. Oliver, A.E. Huespe, and P.J. Sánchez, A comparative study on finite elements for capturing strong discontinuities: E -FEM vs X-FEM, *Comput. Methods Appl. Mech. Eng.*, vol. 195, no. 37–40, pp. 4732–4752, 2006. DOI: [10.1016/j.cma.2005.09.020](https://doi.org/10.1016/j.cma.2005.09.020).
- [10] C. Linder, and F. Armero, Finite elements with embedded strong discontinuities for the modeling of failure in solids, *Int. J. Numer. Meth. Eng.*, vol. 72, no. 12, pp. 1391–1433, 2007. DOI: [10.1002/nme.2042](https://doi.org/10.1002/nme.2042).
- [11] A. Earij, G. Alfano, K. Cashell, and X. Zhou, Nonlinear three-dimensional finite-element modelling of reinforced-concrete beams: computational challenges and experimental validation, *Eng. Fail. Anal.*, vol. 82, pp. 92–115, 2017. DOI: [10.1016/j.engfailanal.2017.08.025](https://doi.org/10.1016/j.engfailanal.2017.08.025).
- [12] M. Kurumatani, Y. Soma, and K. Terada, Simulations of cohesive fracture behavior of reinforced concrete by a fracture-mechanics-based damage model, *Eng. Fract. Mech.*, vol. 206, pp. 392–407, 2019. DOI: [10.1016/j.engfracmech.2018.12.006](https://doi.org/10.1016/j.engfracmech.2018.12.006).
- [13] M.C. Gurtin, E. Fried, and L. Anand, *The Mechanics and Thermodynamics of Continua*, Cambridge University Press, Cambridge, UK, 2010.
- [14] J. Mazars, *Application de la mécanique de l'endommagement au comportement non linéaire et à la rupture du béton de structure*, PhD thesis, Université Pierre et Marie Curie Paris 6, Paris, France, 1984.
- [15] D. Halm, and A. Dragon, A model of anisotropic damage by mesocrack growth; unilateral effect, *Int. J. Damage Mech.*, vol. 5, no. 4, pp. 384–402, 1996. DOI: [10.1177/105678959600500403](https://doi.org/10.1177/105678959600500403).
- [16] J. Lee, and G.L. Fenves, Plastic-damage model for cyclic loading of concrete structures, *J. Eng. Mech.*, vol. 124, no. 8, pp. 892–900, 1998. DOI: [10.1061/\(ASCE\)0733-9399\(1998\)124:8\(892\)](https://doi.org/10.1061/(ASCE)0733-9399(1998)124:8(892)).
- [17] J.Y. Wu, J. Li, and R. Faria, An energy release rate-based plastic-damage model for concrete, *Int. J. Solids Struct.*, vol. 43, no. 3–4, pp. 583–612, 2006. DOI: [10.1016/j.ijsolstr.2005.05.038](https://doi.org/10.1016/j.ijsolstr.2005.05.038).
- [18] Z.P. Bažant, Instability, ductility, and size effect in strain-softening concrete, *J. Engrg. Mech. Div.*, vol. 102, no. 2, pp. 331–344, 1976. DOI: [10.1061/JMCEA3.0002111](https://doi.org/10.1061/JMCEA3.0002111).
- [19] G. Borino, B. Failla, and F. Parrinello, A symmetric nonlocal damage theory, *Int. J. Solids Struct.*, vol. 40, no. 13–14, pp. 3621–3645, 2003. DOI: [10.1016/S0020-7683\(03\)00144-6](https://doi.org/10.1016/S0020-7683(03)00144-6).
- [20] R.H.J. Peerlings, M.G.D. Geers, R.R. De Borst, and W.A.M. Brekelmans, A critical comparison of nonlocal and gradient-enhanced softening continua, *Int. J. Solids Struct.*, vol. 38, no. 44–45, pp. 7723–7746, 2001. DOI: [10.1016/S0020-7683\(01\)00087-7](https://doi.org/10.1016/S0020-7683(01)00087-7).
- [21] Z.P. Bažant, and B.H. Oh, Crack band theory for fracture of concrete, *Mat. Constr.*, vol. 16, no. 3, pp. 155–177, 1983. DOI: [10.1007/BF02486267](https://doi.org/10.1007/BF02486267).
- [22] M. Jirásek, and M. Bauer, Numerical aspects of the crack band approach, *Comput. Struct.*, vol. 110–111, pp. 60–78, 2012. DOI: [10.1016/j.compstruc.2012.06.006](https://doi.org/10.1016/j.compstruc.2012.06.006).
- [23] M. Suidan, and W.C. Schnobrich, Finite element analysis of reinforced concrete, *J. Struct. Div.*, vol. 99, no. 10, pp. 2109–2122, 1973. DOI: [10.1061/JSDIAG.0003623](https://doi.org/10.1061/JSDIAG.0003623).
- [24] H. Sinaei, M. Shariati, A.H. Abna, M. Aghaei, and A. Shariati, Evaluation of reinforced concrete beam behaviour using finite element analysis by ABAQUS, *Sci. Res. Essays.*, vol. 7, no. 21, pp. 2002–2009, 2012.
- [25] A. Casanova, L. Jason, and L. Davenne, Bond slip model for the simulation of reinforced concrete structures, *Eng. Struct.*, vol. 39, pp. 66–78, 2012. DOI: [10.1016/j.engstruct.2012.02.007](https://doi.org/10.1016/j.engstruct.2012.02.007).
- [26] J. Murcia-Delso, and P. Benson Shing, Bond-slip model for detailed finite-element analysis of reinforced concrete structures, *J. Struct. Eng.*, vol. 141, no. 4, p. 04014125, 2015. DOI: [10.1061/\(ASCE\)ST.1943-541X.0001070](https://doi.org/10.1061/(ASCE)ST.1943-541X.0001070).
- [27] C. Combesure, H. Dumontet, and F. Voldoire, Dissipative homogenised reinforced concrete (DHRC) constitutive model dedicated to reinforced concrete plates under seismic loading, *Int. J. Solids Struct.*, vol. 73–74, pp. 78–98, 2015. DOI: [10.1016/j.ijsolstr.2015.07.007](https://doi.org/10.1016/j.ijsolstr.2015.07.007).
- [28] A. Drougkas, V. Sarhosis, and G. Thermou, Micromechanical homogenisation of steel bars in reinforced concrete for damage analysis, *Mater. Today Commun.*, vol. 31, p. 103235, 2022. DOI: [10.1016/j.mtcomm.2022.103235](https://doi.org/10.1016/j.mtcomm.2022.103235).
- [29] E. Carrera, G. Giunta, and M. Petrolo, *Beam Structures: Classical and Advanced Theories*, John Wiley & Sons, Chichester, UK, 2011.
- [30] M. Petrolo, E. Carrera, M. Cinefra, and E. Zappino, *Finite Element Analysis of Structures through Unified Formulation*, John Wiley & Sons, Chichester, UK, 2014.
- [31] E. Carrera, M. Filippi, and E. Zappino, Laminated beam analysis by polynomial, trigonometric, exponential and zig-zag theories, *Eur. J. Mech.-A/Solids*, vol. 41, pp. 58–69, 2013. DOI: [10.1016/j.euromechsol.2013.02.006](https://doi.org/10.1016/j.euromechsol.2013.02.006).
- [32] A. Pagani, E. Carrera, R. Augello, and D. Scano, Use of Lagrange polynomials to build refined theories for laminated beams, plates and shells, *Compos. Struct.*, vol. 276, pp. 114505, 2021. DOI: [10.1016/j.compstruct.2021.114505](https://doi.org/10.1016/j.compstruct.2021.114505).
- [33] J. Shen, A. Pagani, M.R.T. Arruda, and E. Carrera, Exact component-wise solutions for 3d free vibration and stress analysis of hybrid steel-concrete composite beams, *Thin. Walled Struct.*, vol. 174, pp. 109094, 2022. DOI: [10.1016/j.tws.2022.109094](https://doi.org/10.1016/j.tws.2022.109094).
- [34] M.R.T. Arruda, L.M.S. Castro, A.J.M. Ferreira, D. Martins, and J.R. Correia, Physically non-linear analysis of beam models using Carrera Unified Formulation, *Compos. Struct.*, vol. 195, pp. 60–73, 2018. DOI: [10.1016/j.compstruct.2018.03.107](https://doi.org/10.1016/j.compstruct.2018.03.107).
- [35] I. Kaleel, M. Petrolo, A.M. Waas, and E. Carrera, Micromechanical progressive failure analysis of fiber-reinforced composite using refined beam models, *Trans. ASME, J. Appl. Mech.*, vol. 85, no. 2, pp. 021004, 2018. DOI: [10.1115/1.4038610](https://doi.org/10.1115/1.4038610).
- [36] E. Carrera, R. Augello, A. Pagani, and X. Xu, Component-wise approach to reinforced concrete structures, *Mech. Adv. Mater. Struct.*, vol. 29, no. 25, pp. 3871–3888, 2022. DOI: [10.1080/15376494.2021.1912442](https://doi.org/10.1080/15376494.2021.1912442).
- [37] M. Nagaraj, and M. Maiaru, Progressive damage analysis of steel-reinforced concrete beams using higher-order 1d finite

- elements, *Int. J. Multiscale Comput. Eng.*, vol. 21, no. 4, pp. 57–65, 2023. DOI: [10.1615/IntJMultCompEng.2022045649](https://doi.org/10.1615/IntJMultCompEng.2022045649).
- [38] M.R.T. Arruda, J. Pacheco, L.M.S. Castro, and F. Julio, A modified Mazars damage model with energy regularization, *Eng. Fract. Mech.*, vol. 259, p. 108129, 2022. DOI: [10.1016/j.engfrac-mech.2021.108129](https://doi.org/10.1016/j.engfrac-mech.2021.108129).
- [39] J. Shen, M.R.T. Arruda, and A. Pagani, Concrete damage analysis based on higher-order beam theories using fracture energy regularization, *Mech. Adv. Mater. Struct.*, vol. 30, no. 22, pp. 4582–4596, 2023. DOI: [10.1080/15376494.2022.2098430](https://doi.org/10.1080/15376494.2022.2098430).
- [40] fib special activity group, *New Model Code and Taerwe, Luc and Matthys, Stijn, Fib Model Code for Concrete Structures 2010*, Ernst & Sohn, Wiley, Lausanne, Switzerland, 2013.
- [41] EN, EN 1992-1-1 Eurocode 2: Design of Concrete structures - Part 1-1: General Rules and Rules for Buildings, CEN, Brussels, Belgium, 2005.
- [42] J.G. Rots, Computational modeling of concrete fracture, PhD thesis, Delft University of Technology, Delft, Netherlands, 1988.
- [43] V. Cervenka, Mesh sensitivity effects in smeared finite element analysis of concrete fracture, in *FRAMCOS-2*, pp. 1387–1396, 1995.
- [44] J. Oliver, A consistent characteristic length for smeared crack-ing models, *Int. J. Numer. Methods Eng.*, vol. 28, no. 2, pp. 461–474, 1989. DOI: [10.1002/nme.1620280214](https://doi.org/10.1002/nme.1620280214).
- [45] S. Govindjee, G.J. Kay, and J.C. Simo, Anisotropic modelling and numerical simulation of brittle damage in concrete, *Int. J. Numer. Methods Eng.*, vol. 38, no. 21, pp. 3611–3633, 1995. DOI: [10.1002/nme.1620382105](https://doi.org/10.1002/nme.1620382105).
- [46] A.T. Slobbe, M.A.N. Hendriks, and J.G. Rots, Systematic assess-ment of directional mesh bias with periodic boundary conditions: applied to the crack band model, *Eng. Fract. Mech.*, vol. 109, pp. 186–208, 2013. DOI: [10.1016/j.engfracmech.2013.06.005](https://doi.org/10.1016/j.engfracmech.2013.06.005).
- [47] W. He, Y. Xu, Y. Cheng, P.F. Jia, and T.T. Fu, Tension-com-pression damage model with consistent crack bandwidths for concrete materials, *Adv. Civ. Eng.*, vol. 2019, pp. 1–16, 2019. DOI: [10.1155/2019/2810108](https://doi.org/10.1155/2019/2810108).
- [48] J. Shen, A. Pagani, and M.R.T. Arruda, A consistent crack bandwidth for higher-order beam theories: application to concrete.
- [49] F. Leonhardt, and R. Walther, *Schubversuche an einfeldrigen Stahlbetonbalken mit und ohne Schubbewehrung zur Ermittlung der Schubtragfähigkeit und der oberen Schubspannungsgrenze*, Ernst, Berlin, 1962.
- [50] J.P. Firmo, M.R.T. Arruda, and J.R. Correia, Numerical simula-tion of the fire behaviour of thermally insulated reinforced con-crete beams strengthened with EBR-CFRP strips, *Compos. Struct.*, vol. 126, pp. 360–370, 2015. DOI: [10.1016/j.compstruct.2015.02.084](https://doi.org/10.1016/j.compstruct.2015.02.084).
- [51] J.P. Firmo, M.R.T. Arruda, J.R. Correia, and I.C. Rosa, Three-dimensional finite element modelling of the fire behaviour of insulated rc beams strengthened with ebr and nsm cfrp strips, *Compos. Struct.*, vol. 183, pp. 124–136, 2018. DOI: [10.1016/j.compstruct.2017.01.082](https://doi.org/10.1016/j.compstruct.2017.01.082).
- [52] D. Lau, and H.J. Pam, Experimental study of hybrid frp rein-forced concrete beams, *Eng. Struct.*, vol. 32, no. 12, pp. 3857–3865, 2010. DOI: [10.1016/j.engstruct.2010.08.028](https://doi.org/10.1016/j.engstruct.2010.08.028).
- [53] E. Carrera, and E. Zappino, One-dimensional finite element for-mulation with node-dependent kinematics, *Comput. Struct.*, vol. 192, pp. 114–125, 2017. DOI: [10.1016/j.compstruc.2017.07.008](https://doi.org/10.1016/j.compstruc.2017.07.008).